

# JCTC

Journal of Chemical Theory and Computation

## Metal–Metal Quintuple and Sextuple Bonding in Bent Dimetalloenes of the Third Row Transition Metals

Bing Xu,<sup>†,‡</sup> Qian-Shu Li,<sup>\*,‡,§</sup> Yaoming Xie,<sup>||</sup> R. Bruce King,<sup>\*,§,||</sup> and Henry F. Schaefer III<sup>||</sup>

*Beijing University of Posts and Telecommunication, Beijing 100876, China, Institute of Chemical Physics, Beijing Institute of Technology, Beijing 100081, China, Center for Computational Quantum Chemistry, South China Normal University, Guangzhou, 510631 China, and Department of Chemistry and Center for Computational Chemistry, University of Georgia, Athens, Georgia 30602*

Received October 23, 2009

**Abstract:** Theoretical studies on the dimetalloenes  $\text{Cp}_2\text{M}_2$  ( $\text{M} = \text{Os}, \text{Re}, \text{W}, \text{Ta}$ ) predict bent structures with short metal–metal distances suggesting high-order metal–metal multiple bonds. Analysis of the frontier bonding molecular orbitals indicates a formal Os–Os quintuple bond ( $\sigma + 2\pi + 2\delta$ ) in singlet  $\text{Cp}_2\text{Os}_2$  and a formal Re–Re sextuple bond ( $2\sigma + 2\pi + 2\delta$ ) in singlet  $\text{Cp}_2\text{Re}_2$ , thereby giving the metals in both molecules the favored 18-electron metal configurations. Predicted low-energy triplet structures for  $\text{Cp}_2\text{M}_2$  ( $\text{M} = \text{Os}, \text{Re}$ ) have formal quintuple bonds but with only two  $\delta$  one-electron “half” bonds ( $\text{M} = \text{Os}$ ) or a single  $\delta$  two-electron bond ( $\text{M} = \text{Re}$ ) and a second  $\sigma$  component derived from overlap of the  $d(z^2)$  orbitals. A quintuple bond similar to that found in triplet  $\text{Cp}_2\text{Re}_2$  is found in singlet  $\text{Cp}_2\text{W}_2$ , giving both tungsten atoms a 16-electron configuration. The formal Ta–Ta quadruple bond in the lowest energy singlet  $\text{Cp}_2\text{Ta}_2$  structure is different from that in the original  $\text{Re}_2\text{Cl}_8^{2-}$  in that it is a  $2\sigma + 2\pi$  bond with no  $\delta$  components but only  $\sigma$  and  $\pi$  components.

### 1. Introduction

The chemistry of metal–metal multiple bonding<sup>1,2</sup> dates back to the pioneering work of Cotton and Harris<sup>3</sup> in 1965 on the rhenium–rhenium quadruple bond in the binuclear metal halide complex  $\text{Re}_2\text{Cl}_8^{2-}$ . This was not only the first example of a metal–metal quadruple bond but also the first example of a quadruple bond of any type. The highest known formal metal–metal bond order in a stable molecule then remained four for 40 years until the 2005 discovery by Power et al.<sup>4</sup> of a binuclear chromium(I) aryl of the type  $\text{RCrCrR}$ , with an extremely short metal–metal distance, suggesting a formal quintuple bond. This seminal discovery stimulated numerous theoretical

studies on high order metal–metal bonds.<sup>5–11</sup> In addition, various research groups reported further experimental work on low oxidation state transition metal aryls of the type  $\text{RMMR}$ <sup>12,13</sup> as well as chromium(I) amidinate,<sup>14,15</sup> 2-aminopyridine,<sup>16</sup> and diazadiene<sup>17</sup> complexes, apparently containing formal quintuple bonds.

Another key development in organometallic chemistry in recent years has been the synthesis of formal  $\text{Zn(I)}$  derivatives with direct  $\text{Zn–Zn}$  bonds.<sup>18,19</sup> Such compounds include dizincocene,  $\text{CpZn–ZnCp}$  ( $\text{Cp} = \eta^5\text{-C}_5\text{H}_5$ ), in which two  $\text{CpZn}$  units are linked by a direct zinc–zinc single bond of length 2.305 Å to give both zinc atoms the favored 18-electron configuration.<sup>18</sup> Simple electron counting guided by the 18-electron rule suggests that analogous dimetalloenes of earlier transition metals could provide interesting new examples of metal–metal multiple bonding. The stability of  $\text{Re}_2\text{Cl}_8^{2-}$  with a formal rhenium–rhenium quadruple bond<sup>3</sup> suggests that the best candidates for stable dimetalloenes with interesting metal–metal mul-

\* Corresponding author e-mail: rbking@chem.uga.edu (R.B.K.) and qsl@scnu.edu.cn (Q.-S.L.).

<sup>†</sup> Beijing University of Posts and Telecommunication.

<sup>‡</sup> Beijing Institute of Technology.

<sup>§</sup> South China Normal University.

<sup>||</sup> University of Georgia.

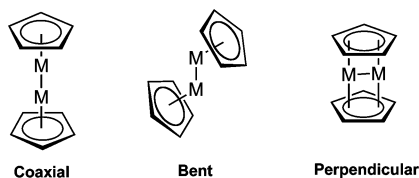


**Figure 1.** Three types of dimetalloocene structures.

tiple bonds might contain the heaviest transition metals, particularly those of the third row.

These considerations led us to investigate dimetalloenes  $\text{Cp}_2\text{M}_2$  of the early transition metals of the third row ( $\text{M} = \text{Os}, \text{Re}, \text{W}, \text{Ta}$ ) as candidates for new types of molecules with high order metal–metal bonds. In this connection, all of these dimetalloenes were found by density functional theory (DFT) to exhibit bent structures in contrast to the coaxial structure found<sup>18</sup> for  $\text{Cp}_2\text{Zn}_2$  and the perpendicular structures for late transition metal metallocenes predicted by theory in 2005 (Figure 1).<sup>20</sup>

The theoretical studies of the dimetalloenes  $\text{Cp}_2\text{M}_2$  ( $\text{M} = \text{Os}, \text{Re}, \text{W}, \text{Ta}$ ) discussed in this paper consist of two phases: (1) optimizations of structures with singlet, triplet, and quintet spin states using density functional methods and (2) elucidation of the formal metal–metal bond orders in the lowest energy optimized structures by analysis of the highest occupied molecular orbitals (MOs). The MO studies provide more direct evidence for the high order metal–metal multiple bonds, already suggested by the relatively short metal–metal distances. Thus, evidence is provided for the formal osmium–osmium quintuple bond in  $\text{Cp}_2\text{Os}_2$  required to give both osmium atoms the favored 18-electron rare gas configuration.

## 2. Theoretical Methods

Electron correlation effects were considered by employing density functional theory (DFT), which has evolved as a practical and effective computational tool, especially for organometallic compounds.<sup>21–35</sup> In this research, two DFT methods, BP86 and MPW1PW91, were used. The BP86 method is a pure DFT method that combines Becke's 1988 exchange functional with Perdew's 1986 correlation functional.<sup>36,37</sup> The MPW1PW91 method<sup>38</sup> is a so-called second generation<sup>39</sup> functional, which combines the modified Perdew–Wang exchange functional with Perdew–Wang's 1991 correlation functional.<sup>40</sup> The MPW1PW91 method has been found to be typically more suitable for geometry optimization of the second and third row transition metal systems,<sup>41,42</sup> while the BP86 method usually provides better vibrational frequencies with DZP basis sets.

For the third row transition metals, the large numbers of electrons may increase exponentially the computational efforts. In order to reduce the cost, effective core potential (ECP) relativistic basis sets are employed. The SDD (Stuttgart–Dresden ECP plus DZ)<sup>43</sup> ECP basis set was used for the Os, Re, W, and Ta atoms. For the C atom, the double- $\zeta$  plus polarization (DZP) basis set was used. The latter are the Huzinaga–Dunning contracted double- $\zeta$  sets<sup>44,45</sup> plus a set of spherical harmonic d polarization functions with an orbital exponent  $\alpha_d(\text{C}) = 0.75$ , designated as (9s5p1d/

4s2p1d). For H, a set of p polarization functions,  $\alpha_p(\text{H}) = 0.75$ , was added to the Huzinaga–Dunning DZ set.

The geometries of all structures were fully optimized using the two selected DFT methods with the SDD ECP basis set. The vibrational frequencies were determined by evaluating analytically the second derivatives of the energy with respect to the nuclear coordinates at the same theoretical levels. The corresponding infrared intensities were also evaluated analytically.

All of the computations were carried out with the Gaussian 03 program.<sup>46</sup> The fine (75, 302) grid is the default for evaluating integrals numerically, and the tight ( $10^{-8}$  hartree) designation is the default for the energy convergence. The finer grid (120, 974) was used for more carefully characterizing small imaginary vibrational frequencies.

## 3. Results

### 3.1. $\text{Cp}_2\text{M}_2$ ( $\text{M} = \text{Os}, \text{Re}, \text{W}, \text{Ta}$ ) Structures.

**3.1.1.  $\text{Cp}_2\text{Os}_2$ .** Initially, we investigated the linear  $D_{5h}$  and  $D_{5d}$  structures of  $\text{Cp}_2\text{Os}_2$ , which are similar to the experimental  $\text{Cp}_2\text{Zn}_2$  structure.<sup>18</sup> However, these structures were found to have four imaginary vibrational frequencies at  $160i$ ,  $160i$ ,  $56i$ , and  $56i$   $\text{cm}^{-1}$  (for  $D_{5h}$ ) or  $160i$ ,  $160i$ ,  $56i$ , and  $56i$   $\text{cm}^{-1}$  (for  $D_{5d}$ ). Following the corresponding normal modes leads to the bent  $C_{2h}$  structure Os–S, which lies below the two linear structures by  $\sim 49$  kcal/mol.

The bent  $C_{2h}$  singlet structure Os–S (Figure 2 and Table 1) is the global minimum. The Os–Os distance in Os–S is predicted to be 2.333 Å (MPW1PW91) or 2.276 Å (BP86). This is short enough to correspond to the formal quintuple bond required to give both osmium atoms the favored 18-electron configuration. Furthermore, the Os–Os distance in Os–S is  $\sim 0.5$  Å shorter than the experimental Os–Os single bond distance of 2.767 Å in  $(\eta^5\text{-Me}_5\text{C}_5)_2\text{Os}_2(\text{CO})_2(\mu\text{-CO})_2$  determined by X-ray crystallography.<sup>47</sup>

The triplet structure Os–T for  $\text{Cp}_2\text{Os}_2$  (Figure 2) is predicted to lie only 0.1 kcal/mol (MPW1PW91) lower or 3.6 kcal/mol (BP86) higher in energy than the singlet structure Os–S (Table 1). A small imaginary vibrational frequency at  $67i$   $\text{cm}^{-1}$  is predicted by the MPW1PW91 method, while all real vibrational frequencies are predicted by the BP86 method. The  $67i$   $\text{cm}^{-1}$  imaginary vibrational frequency cannot be removed by using a finer integration grid (120, 974). Following the corresponding normal mode of the imaginary vibrational frequency leads to a  $C_1$  structure, which only slightly deviates from the  $C_2$  structure Os–T. The Os–Os bond length in Os–T is predicted to be 2.277 Å (MPW1PW91) or 2.255 Å (BP86).

The quintet structure Os–Q for  $\text{Cp}_2\text{Os}_2$  ( $C_2$ ) is predicted to have all real vibrational frequencies by both DFT methods and lies 6.7 kcal/mol (MPW1PW91) or 17.0 kcal/mol (BP86) higher in energy than the singlet structure Os–S (Table 1). The Os–Os bond length in Os–Q is predicted to be essentially the same as Os–T, namely, 2.281 Å (MPW1PW91) or 2.290 Å (BP86), respectively. Note that all three Os–Os distances are essentially the same for the three  $\text{Cp}_2\text{Os}_2$  structures Os–S, Os–T, and Os–Q regardless of the spin state.

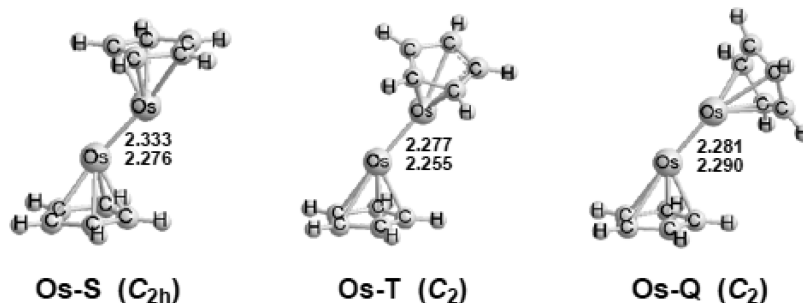


**Figure 2.** Optimized structures for  $\text{Cp}_2\text{Os}_2$ . Distances are reported in Å. The upper distances were predicted by the MPW1PW91 method and the lower distances by the BP86 method (same for subsequent figures).

**Table 1.** Total Energies ( $E$ , in Hartree), Relative Energies ( $\Delta E$ , in kcal/mol), Numbers of Imaginary Vibrational Frequencies (Nimag), Os–Os Bond Distances (Å), and Spin Expectation Values ( $\langle S^2 \rangle$ ) for the Optimized  $\text{Cp}_2\text{Os}_2$  Structures

		Os–S ( $C_{2h}$ )	Os–T ( $C_2$ )	Os–Q ( $C_2$ )
	state	$^1A_g$	$^3B$	$^5A$
MPW1PW91	$E$	−568.42221	−568.42243	−568.41160
	$\Delta E$	0.0	−0.1	6.7
	Nimag	0	1(67)	0
	Os–Os	2.333	2.277	2.281
	$\langle S^2 \rangle$	0	2.02	6.03
BP86	$E$	−568.71958	−568.71385	−568.69253
	$\Delta E$	0.0	3.6	17.0
	Nimag	0	0	0
	Os–Os	2.276	2.255	2.290
	$\langle S^2 \rangle$	0	2.01	6.02

**3.1.2.  $\text{Cp}_2\text{Re}_2$ .** The global minimum of  $\text{Cp}_2\text{Re}_2$  is predicted to be a  $C_2$  triplet *trans* structure  $\text{Re–T}_1$  (Figure 3 and Table 2) with all real vibrational frequencies by the MPW1PW91 method but with a very small imaginary vibrational frequency at  $18i \text{ cm}^{-1}$  by the BP86 method. This imaginary vibrational frequency is removed by using a finer integration grid (120, 974), indicating that it is caused by numerical integration error. The Re–Re distance in  $\text{Re–T}_1$  is predicted to be very short at 2.323 Å (MPW1PW91) or 2.272 Å (BP86), suggesting a metal–metal bond of high multiplicity. In this connection, the formal  $\text{Re}\equiv\text{Re}$  triple bond in  $(\eta^5\text{-Me}_5\text{C}_5)_2\text{Re}_2(\mu\text{-CO})_3$  is found experimentally by X-ray diffraction<sup>48</sup> to be 2.411 Å, suggesting on the basis of bond length a formal bond order appreciably greater than three for the appreciably shorter Re–Re bond in  $\text{Re–T}_1$ . A related *cis*  $C_2$  triplet  $\text{Cp}_2\text{Re}_2$  structure  $\text{Re–T}_2$  (Figure 3 and Table 2) is also predicted to be a genuine minimum, lying only 0.9 kcal/mol (MPW1PW91) or 2.3 kcal/mol (BP86) above the global minimum  $\text{Re–T}_1$ .

A singlet  $\text{Cp}_2\text{Re}_2$  structure  $\text{Re–S}$  (Figure 3 and Table 2) is predicted at 8.0 kcal/mol (MPW1PW91) or 0.6 kcal/mol (BP86) in energy above  $\text{Re–T}_1$  with all real vibrational frequencies. The Re–Re distance in  $\text{Re–S}$  is predicted to be even 0.08 Å shorter than the already very short Re–Re distance in  $\text{Re–T}_1$ . This is consistent with the requirement in  $\text{Cp}_2\text{Re}_2$  of a formal quintuple bond to give the rhenium atoms in  $\text{Cp}_2\text{Re}_2$  the 17-electron rhenium configurations in the binuclear triplet  $\text{Re–T}_1$  but a formal sextuple bond for the favored 18-electron rhenium configurations in the singlet  $\text{Re–S}$ .

The  $C_{2h}$  symmetry quintet  $\text{Cp}_2\text{Re}_2$  structure  $\text{Re–Q}_3$  (Figure 3 and Table 2) is predicted to lie 2.3 kcal/mol (MPW1PW91) or 8.8 kcal/mol (BP86) higher in energy than the global minimum  $\text{Re–T}_1$ . The MPW1PW91 method predicts all real vibrational frequencies for  $\text{Re–Q}_3(C_{2h})$ , while a substantial imaginary vibrational frequency at  $142i \text{ cm}^{-1}$  is predicted by the BP86 method. Following the corresponding normal mode of this imaginary vibrational frequency leads to structure  $\text{Re–Q}_1(C_i)$  (Figure 3), which is 1.2 kcal/mol (BP86) lower in energy than  $\text{Re–Q}_3$  (Table 2). A *cis*  $\text{Cp}_2\text{Re}_2$  quintet  $C_2$  structure  $\text{Re–Q}_2$  (Figure 3 and Table 2) is predicted to lie 0.9 kcal/mol (BP86) higher in energy than  $\text{Re–Q}_1(C_i)$ . The Re–Re bond lengths in  $\text{Re–Q}_1$  and  $\text{Re–Q}_2$  are almost the same at 2.305 Å (BP86), whereas a slightly longer Re–Re bond at 2.339 Å (BP86) is predicted for structure  $\text{Re–Q}_3$ . Since unstable electronic states could be the computational results for the bimetallic systems and  $\text{Re–Q}_1$  and  $\text{Re–Q}_2$  are two prime candidates for this problem, we checked the stability for these two structures. However, our results confirm that they are both stable.

**3.1.3.  $\text{Cp}_2\text{W}_2$ .** The  $C_2$  singlet  $\text{Cp}_2\text{W}_2$  structure  $\text{W–S}$  (Figure 4 and Table 3) is predicted to be the global minimum of  $\text{Cp}_2\text{W}_2$  by the BP86 method. The triplet and quintet structures of  $\text{Cp}_2\text{W}_2$  are predicted by BP86 to lie 9.0 and 10.3 kcal/mol, respectively, higher in energy than  $\text{W–S}$  (Table 3). However, the  $C_2$  quintet structure  $\text{W–Q}$  is predicted to be the global minimum for  $\text{Cp}_2\text{W}_2$  by MPW1PW91 at just 1.4 kcal/mol lower in energy than  $\text{W–S}$ . All four  $\text{Cp}_2\text{W}_2$  structures are found to have all real vibrational frequencies by BP86. Whereas, the  $\text{Cp}_2\text{W}_2$  structures  $\text{W–S}$  and  $\text{W–T}_1$  (Figure 4, Table 3) are predicted to have small imaginary vibrational frequencies at  $22i \text{ cm}^{-1}$  ( $\text{W–S}$ ) or  $32i \text{ cm}^{-1}$  ( $\text{W–T}_1$ ) with the MPW1PW91 method (Table 3). These small imaginary vibrational frequencies are not removed by the finer integration grid of (120, 974). Following the corresponding normal modes (Cp ring rotations) of these small imaginary vibrational frequencies led to  $C_1$  structures with essentially unchanged W–W distances and energies lower by only  $\sim 1$  kcal/mol. The triplet structures  $\text{W–T}_1$  and  $\text{W–T}_2$  (Figure 4, Table 3) exhibit significant spin contamination by the MPW1PW91 method, namely,  $\langle S^2 \rangle = 2.33$  and 2.23 versus the ideal  $S(S+1) = 2$ , however, the BP86 method predicts less spin contamination ( $\langle S^2 \rangle = 2.07$  and 2.09) for these two triplet structures. The W–W distances of  $\text{Cp}_2\text{W}_2$  structures are predicted to fall in the range of 2.291 Å to 2.414 Å, consistent with higher order W–W

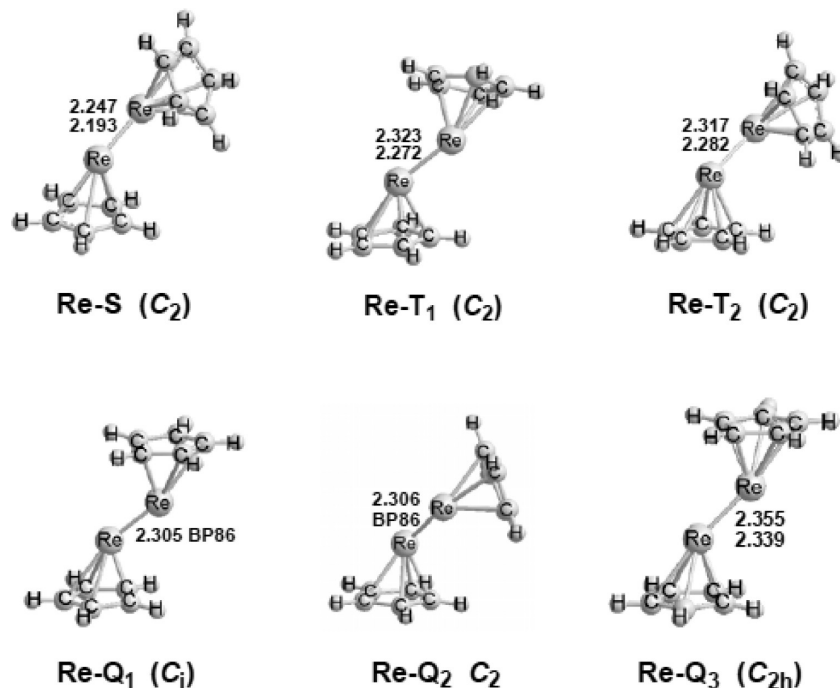


**Figure 3.** Optimized structures of  $\text{Cp}_2\text{Re}_2$ .

**Table 2.** Total Energies ( $E$ , in Hartree), Relative Energies ( $\Delta E$ , in kcal/mol), Numbers of Imaginary Vibrational Frequencies (Nimag), Re–Re Bond Distances (Å), and Spin Expectation Values ( $\langle S^2 \rangle$ ) for the Optimized  $\text{Cp}_2\text{Re}_2$  Structures

		Re–S	Re–T <sub>1</sub>	Re–T <sub>2</sub>	Re–Q <sub>1</sub>	Re–Q <sub>2</sub>	Re–Q <sub>3</sub>
		(C <sub>2</sub> )	(C <sub>2</sub> )	(C <sub>2</sub> )	(C <sub>i</sub> )	(C <sub>2</sub> )	(C <sub>2h</sub> )
state		<sup>1</sup> A	<sup>3</sup> B	<sup>3</sup> B	<sup>5</sup> A <sub>g</sub>	<sup>5</sup> A	<sup>5</sup> B <sub>g</sub>
MPW1PW91	$E$	–543.56593	–543.57860	–543.57723			–543.57497
	$\Delta E$	8.0	0.0	0.9			2.3
	Nimag	0	0	0	same as Re–Q <sub>3</sub> (C <sub>2h</sub> )		0
	Re–Re	2.247	2.323	2.317			2.355
	$\langle S^2 \rangle$	0	2.22	2.03			6.08
BP86	$E$	–543.85837	–543.85931	–543.84719	–543.84579	–543.84579	–543.84533
	$\Delta E$	0.6	0.0	2.3	7.6	8.5	8.8
	Nimag	0	1(18i)	0	0	0	1(142i)
	Re–Re	2.193	2.272	2.282	2.305	2.306	2.339
	$\langle S^2 \rangle$	0	2.04	2.01	6.03	6.08	6.03

multiple bonds. For comparison, the  $\text{W}\equiv\text{W}$  triple bond distance found by X-ray crystallography<sup>49</sup> in  $\text{Cp}_2\text{W}_2(\text{CO})_2(\mu\text{-Ph}_2\text{PCH}_2\text{PPh}_2)$  is 2.514 Å. This suggests formal bond orders greater than three for the  $\text{Cp}_2\text{W}_2$  structures.

**3.1.4.  $\text{Cp}_2\text{Ta}_2$ .** The global minimum of  $\text{Cp}_2\text{Ta}_2$  is predicted to be a  $\text{C}_2$  triplet structure Ta–T, having all real vibrational frequencies (Figure 5, Table 4) and a Ta–Ta bond distance of 2.467 Å (MPW1PW91) or 2.480 Å (BP86). In addition, *trans* and *cis* singlet  $\text{Cp}_2\text{Ta}_2$  structures

Ta–S<sub>1</sub> (C<sub>2h</sub>) and Ta–S<sub>2</sub> (C<sub>2</sub>) are predicted to lie above Ta–T by ~5.7 kcal/mol or ~11.2 kcal/mol by MPW1PW91 but ~0.7 kcal/mol lower or ~4.9 kcal/mol higher in energy by BP86 (Figure 5, Table 4). These two singlet structures are both predicted to be genuine minima, having all real vibrational frequencies. The short Ta–Ta bond lengths at 2.369 Å to 2.417 Å in the singlet  $\text{Cp}_2\text{Ta}_2$  structures are again consistent with higher order multiple bonds.

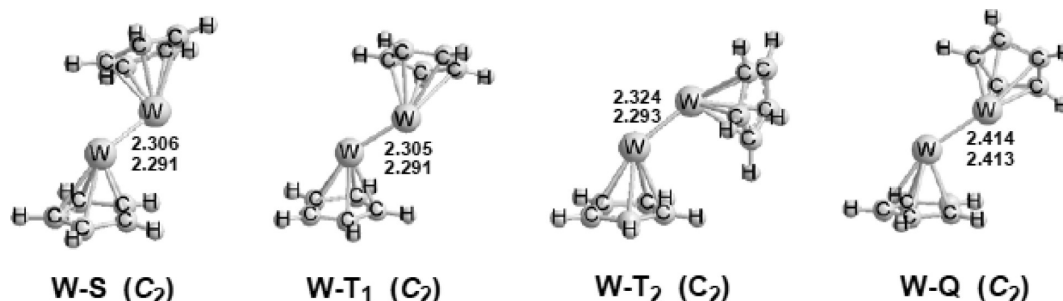


**Figure 4.** Optimized structures of  $\text{Cp}_2\text{W}_2$ .



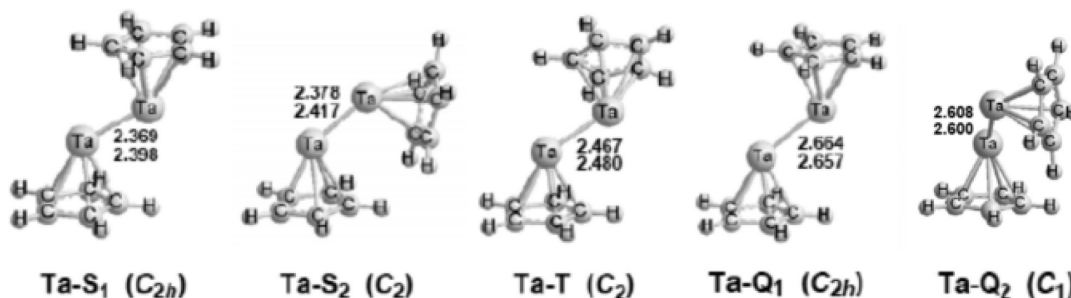
**Table 3.** Total Energies ( $E$ , in Hartree), Relative Energies ( $\Delta E$ , in kcal/mol), Numbers of Imaginary Vibrational Frequencies (Nimag), W–W Bond Distances (Å), and Spin Expectation Values ( $\langle S^2 \rangle$ ) for the Optimized  $\text{Cp}_2\text{W}_2$  Structures

		W–S ( $C_2$ )	W–T <sub>1</sub> ( $C_2$ )	W–T <sub>2</sub> ( $C_2$ )	W–Q ( $C_2$ )
state		<sup>1</sup> A	<sup>3</sup> B	<sup>3</sup> B	<sup>5</sup> A
MPW1PW91	$E$	–521.13768	–521.12591	–521.12455	–521.13991
	$\Delta E$	0.0	7.4	8.2	–1.4
	Nimag	1(22i)	1(32i)	0	0
	W–W	2.306	2.305	2.324	2.414
	$\langle S^2 \rangle$	0	2.33	2.23	6.05
BP86	$E$	–521.40576	–521.39143	–521.38738	–521.38932
	$\Delta E$	0.0	9.0	11.5	10.3
	Nimag	0	0	0	0
	W–W	2.291	2.291	2.293	2.413
	$\langle S^2 \rangle$	0	2.07	2.09	6.02

The *trans* and *cis* quintet structures Ta–Q<sub>1</sub> ( $C_{2h}$ ) and Ta–Q<sub>2</sub> ( $C_1$ ), respectively, are predicted to have all real vibrational frequencies by BP86 (Figure 5, Table 4), while a small imaginary vibrational frequency at 29i cm<sup>–1</sup> for Ta–Q<sub>1</sub> is predicted by MPW1PW91. Following the corresponding normal mode, which corresponds to Cp ring rotation, leads to a  $C_s$  structure with an energy lower by only ~0.2 kcal/mol. The two quintet  $\text{Cp}_2\text{Ta}_2$  structures are predicted to lie in energy above Ta–T by ~6.0 kcal/mol (MPW1PW91) or ~10.5 kcal/mol (BP86). The Ta–Ta distances in Ta–Q<sub>1</sub> and Ta–Q<sub>2</sub> are predicted to fall in the range of 2.600 Å to 2.664 Å, which is ~0.15 to ~0.25 Å longer than those for the singlet and triplet  $\text{Cp}_2\text{Ta}_2$  structures.

**3.2.  $\text{Cp}_2\text{M}_2$  (M = Os, Re, W, Ta) Molecular Orbitals.** The very short M–M bond distances in the  $\text{Cp}_2\text{M}_2$  derivatives (M = Os, Re, W, Ta) suggest metal–metal multiple bonds of relatively high bond orders for practically all of the predicted structures. For singlet  $\text{Cp}_2\text{Os}_2$  and singlet  $\text{Cp}_2\text{Re}_2$ , these metal–metal distances are even short enough to suggest the formal quintuple and sextuple bonds, respec-

tively, required to give both metal atoms the favored 18-electron configurations. In order to obtain further evidence beyond simply very short M–M distances for these very interesting metal–metal multiple bonds in the  $\text{Cp}_2\text{M}_2$  derivatives, their frontier molecular orbitals (MOs) were investigated. The highest occupied molecular orbitals (HOMO) as well as the (typically) five or six orbitals below the HOMO were found to be localized mainly on the metal–metal bonds with relatively little on the Cp rings. These frontier MOs were used to characterize the metal–metal bonding in the dimetalloenes  $\text{Cp}_2\text{M}_2$  (M = Os, Re, W, Ta). In this connection, the formal bond order of the metal–metal bond ( $\text{FBO}_{\text{M–M}}$ ) can be defined by the equation  $\text{FBO}_{\text{M–M}} = \frac{1}{2}(n_{\text{B}} - n_{\text{A}})$  where  $n_{\text{B}}$  and  $n_{\text{A}}$  are the numbers of electrons in the bonding and antibonding orbitals, respectively. The analyses for the all of the optimized  $\text{Cp}_2\text{M}_2$  structures discussed in this paper are summarized in Table 5, along with the M–M bond distances determined by the BP86 method, where data for all of the structures are available. The MOs for the lowest energy  $\text{Cp}_2\text{M}_2$  structures exhibiting metal–metal quintuple

**Figure 5.** Optimized structures of  $\text{Cp}_2\text{Ta}_2$ .**Table 4.** Total Energies ( $E$ , in Hartree), Relative Energies ( $\Delta E$ , in kcal/mol), Numbers of Imaginary Vibrational Frequencies (Nimag), Ta–Ta Bond Distances (Å), and Spin Expectation Values ( $\langle S^2 \rangle$ ) for the Optimized  $\text{Cp}_2\text{Ta}_2$  Structures

		Ta–S <sub>1</sub> ( $C_{2h}$ )	Ta–S <sub>2</sub> ( $C_2$ )	Ta–T ( $C_2$ )	Ta–Q <sub>1</sub> ( $C_{2h}$ )	Ta–Q <sub>2</sub> ( $C_1$ )
state		<sup>1</sup> A <sub>g</sub>	<sup>1</sup> A	<sup>3</sup> B	<sup>5</sup> A <sub>g</sub>	<sup>5</sup> A
MPW1PW91	$E$	–500.97396	–500.96438	–500.98219	–500.97303	–500.97233
	$\Delta E$	5.7	11.2	0.0	5.7	6.2
	Nimag	0	0	0	1(29i)	0
	Ta–Ta	2.369	2.378	2.467	2.664	2.608
	$\langle S^2 \rangle$	0	0	2.01	6.02	6.08
BP86	$E$	–501.21582	–501.20683	–501.21469	–501.19919	–501.19673
	$\Delta E$	–0.7	4.9	0.0	9.7	11.3
	Nimag	0	0	0	0	0
	Ta–Ta	2.398	2.417	2.480	2.657	2.600
	$\langle S^2 \rangle$	0	0	2.01	6.01	6.02

**Table 5.** Formal Metal–Metal Bond Order in the Dimetalocene Structures  $\text{Cp}_2\text{M}_2$  ( $\text{M} = \text{Os}, \text{Re}, \text{W}, \text{Ta}$ ) as Determined by an Analysis of the Bonding Molecular Orbitals

structure	bonding electrons	antibonding electrons	M–M bond order <sup>a</sup> ( $\text{FBO}_{\text{M–M}}$ )	M–M distance, Å (BP86)
<b><math>\text{Cp}_2\text{Os}_2</math></b>				
Os–S	12	2	5	2.276
Os–T	12	2	$4^{2/2}$	2.255
Os–Q	12	2	5	2.290
<b><math>\text{Cp}_2\text{Re}_2</math></b>				
Re–S	12	0	6	2.193
Re–T <sub>1</sub>	11	1	5	2.272
Re–T <sub>2</sub>	11	1	5	2.282
Re–Q <sub>1</sub>	10	2	4	2.305
Re–Q <sub>2</sub>	10	2	4	2.306
Re–Q <sub>3</sub>	10	2	4	2.339
<b><math>\text{Cp}_2\text{W}_2</math></b>				
W–S	10	0	5	2.291
W–T <sub>1</sub>	10	0	$4^{2/2}$	2.291
W–T <sub>2</sub>	10	0	$4^{2/2}$	2.293
W–Q	9	1	4	2.413
<b><math>\text{Cp}_2\text{Ta}_2</math></b>				
Ta–S <sub>1</sub>	8	0	4	2.398
Ta–S <sub>2</sub>	8	0	4	2.417
Ta–T	7	1	3	2.480
Ta–Q <sub>1</sub>	7	1	3	2.657
Ta–Q <sub>2</sub>	7	1	3	2.600

<sup>a</sup> The notation " $2^{1/2}$ " refers to a pair of essentially degenerate one-electron "half bonds."

and sextuple bonding are discussed in detail below. A complete set of the figures of the relevant frontier orbitals of all of the optimized  $\text{Cp}_2\text{M}_2$  structures is given in the Supporting Information.

The M–M bond distances listed in Table 5 show a rough correlation with the formal metal–metal bond order  $\text{FBO}_{\text{M–M}}$  as determined by the numbers of electrons in M–M bonding and M–M antibonding orbitals. Thus, the unique structure with a formal sextuple bond, namely, the singlet  $\text{Cp}_2\text{Re}_2$  structure Re–S, has a Re–Re bond distance of 2.193 Å, which is shorter than any of the other  $\text{Cp}_2\text{M}_2$  derivatives by 0.06 Å or more. The  $\text{Cp}_2\text{M}_2$  derivatives with formal M–M quintuple bonds are predicted to have metal–metal distances in the rather narrow range of 2.25 to 2.29 Å. Comparison of these M–M distances with the 2.222 Å length of the Re–Re quadruple bond in  $\text{Re}_2\text{Cl}_8^{2-}$  found experimentally<sup>50</sup> suggests that Cp ligands lead to longer M–M bonds of a given multiplicity than chloride ligands. The formal M–M quadruple bonds in the  $\text{Cp}_2\text{M}_2$  derivatives are predicted to fall in the range 2.30 to 2.41 Å and thus are significantly longer than the formal Re–Re quadruple bond in  $\text{Re}_2\text{Cl}_8^{2-}$ . The Ta≡Ta triple bonds in the  $\text{Cp}_2\text{Ta}_2$  derivatives Ta–T, Ta–Q<sub>1</sub>, and Ta–Q<sub>2</sub> are still longer at 2.48 to 2.66 Å.

The method of determining the formal bond orders is illustrated for  $\text{Cp}_2\text{Os}_2$  by the singlet structure Os–S (Figures 2 and 6). In this case, the seven highest energy occupied MOs (HOMO down to HOMO–6) have their electron densities concentrated on the metals rather than the rings and thus may be assumed to be responsible for the metal–metal bonding. The lower occupied MOs have most of their electron density on the rings (HOMO–7 to HOMO–10 in Figure 6 and further down) and thus may be related to metal–ring bonding. Among the seven highest occupied MOs, one (HOMO) is clearly antibonding and the other six (HOMO–1 down to HOMO–6) are clearly bonding since

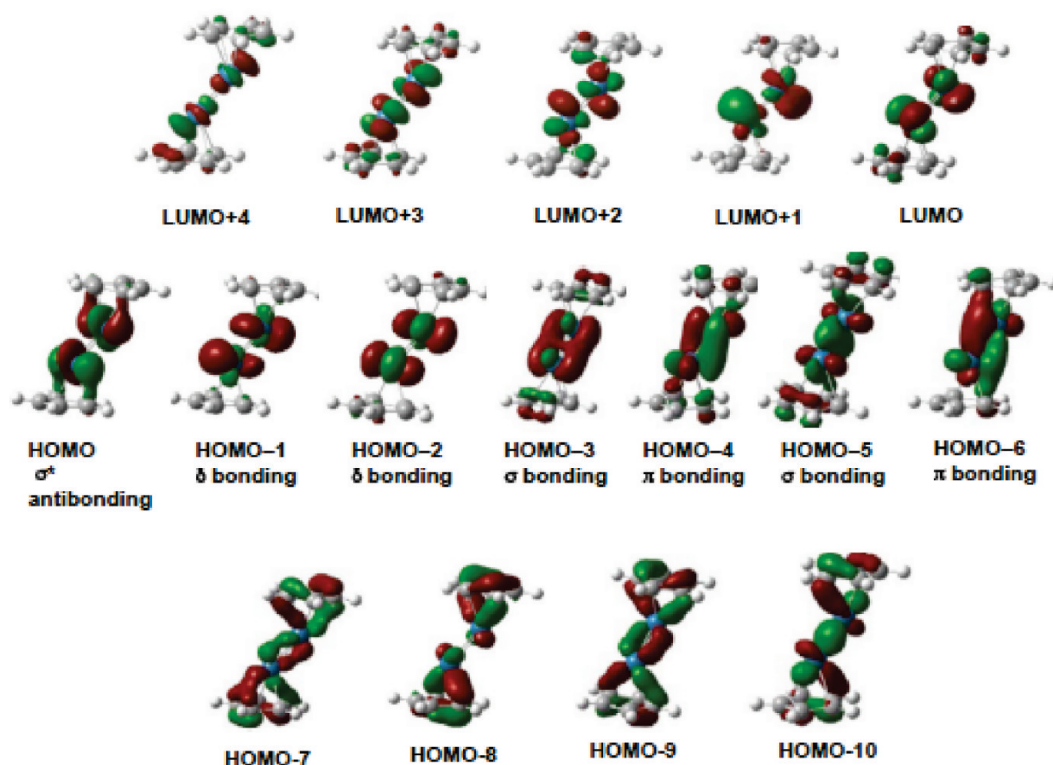


**Figure 6.** The frontier MOs for the singlet structure Os–S of  $\text{Cp}_2\text{Os}_2$ . (a) Top: The unoccupied LUMOs up to LUMO+4. (b) Middle: The occupied HOMOs down to HOMO–6 relating to the osmium–osmium bonding. (c) Bottom: The next lower occupied MOs (HOMO–7 down to HOMO–10), relating largely to the metal–ring bonding.

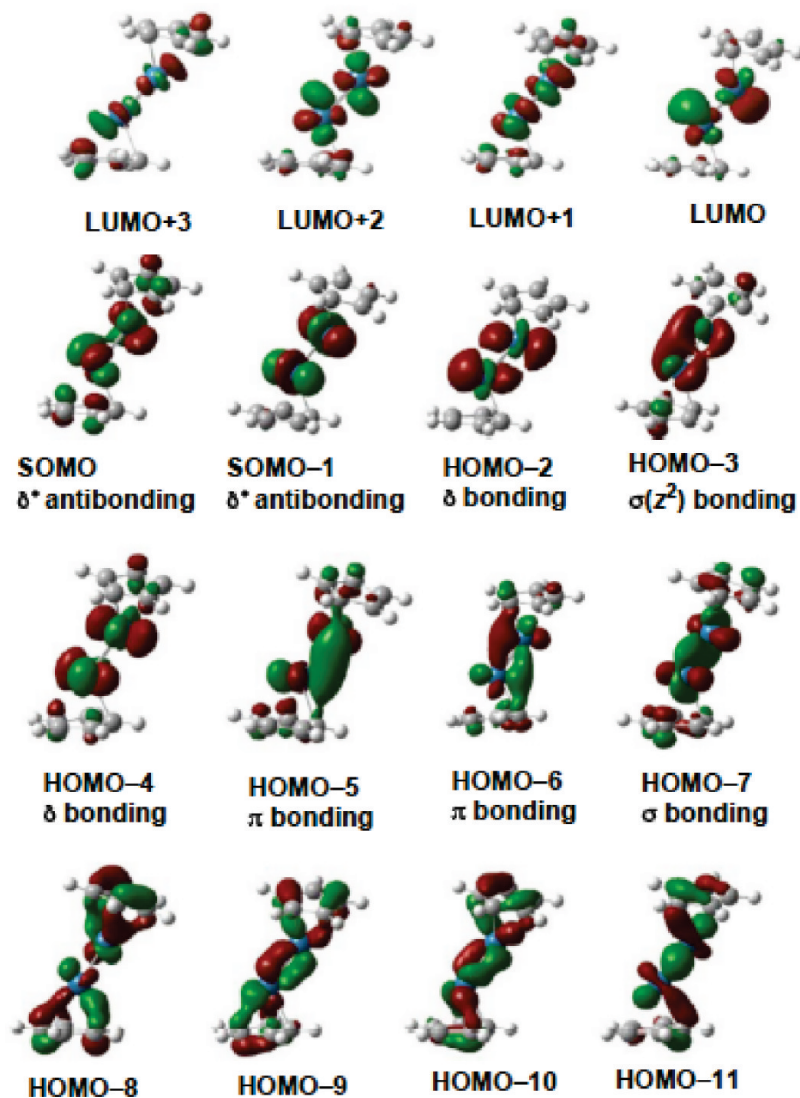


**Figure 7.** The frontier MOs for the triplet structure Os–T of  $\text{Cp}_2\text{Os}_2$ . (a) LUMOs up to LUMO+3 are unoccupied orbitals. (b) SOMO and SOMO–1 are osmium–osmium antibonding orbitals. (c) HOMO–2 to HOMO–7 are osmium–osmium bonding orbitals. (d) Bottom: The next lower occupied MOs (HOMO–8 down to HOMO–11) relate largely to the metal–ring bonding.

there is no node between the metal atoms. This pattern of the occupied MOs (six bonding orbitals and one antibonding orbital) leads to a formal bond order of  $\frac{1}{2}(12 - 2) = 5$ , i.e., the formal quintuple bond needed to give both osmium atoms the favored 18-electron configuration in  $\text{Cp}_2\text{Os}_2$ .

The bent nature of the diosmocene structure Os–S (Figure 2) makes less clear the nature of the components of the osmium–osmium quintuple bond. However, the six bonding orbitals HOMO–1 to HOMO–6 (Figure 6) appear to correspond to two  $\delta$  bonds, a  $\sigma(z^2)$  bond, a  $\pi$  bond, a  $\sigma(s)$  bond, and another  $\pi$  bond, respectively. The filled antibonding orbital (HOMO) appears to be a  $\sigma^*(z^2)$  orbital, thereby canceling out the  $\sigma(z^2)$  bonding component and leaving the five  $\sigma(s) + 2\pi + 2\delta$  bonding components for the quintuple bond, similar to the quintuple bond in the binuclear Cr(I) aryl derivative  $\text{RCrCrR}$  of Power et al.<sup>4</sup> Also, the shapes of the MOs for  $\text{Cp}_2\text{Os}_2$  (Figure 6) indicate the expected weaker overlap in the two  $\delta$  components HOMO–1 and HOMO–2 relative to the  $\sigma$  and  $\pi$  components.

A low energy triplet structure Os–T (Figure 2) is also found for  $\text{Cp}_2\text{Os}_2$ . The frontier molecular orbitals for Os–T

are shown in Figure 7. The two MOs below the LUMO, namely, SOMO and SOMO–1, contain only a single electron corresponding to the triplet spin multiplicity of Os–T. Both of these orbitals correspond to  $\delta^*$  antibonding orbitals. The next six orbitals below SOMO–1, namely, HOMO–2 through HOMO–7, each contain electron pairs and correspond to a  $\delta$  bonding orbital, a  $\sigma(z^2)$  bonding orbital, another  $\delta$  bonding orbital, two  $\pi$  bonding orbitals, and a  $\sigma$  bonding orbital. Thus, the eight orbitals from SOMO down to HOMO–7 correspond to an Os–Os quintuple bond consisting of  $2\sigma + 2\pi$  full bonds and two  $\delta$  half bonds, i.e., a bond of order  $4\frac{1}{2}$ . This is analogous to the well-known bond of order  $1\frac{1}{2}$  in normal (triplet) dioxygen except that in dioxygen the half bonds are  $\pi$  bonds rather than the  $\delta$  bonds in structure Os–T of  $\text{Cp}_2\text{Os}_2$ . Thus, both singlet  $\text{Cp}_2\text{Os}_2$  (Os–S) and triplet  $\text{Cp}_2\text{Os}_2$  (Os–T) have metal–metal bonds of order 5 to give the osmium atoms the favored 18-electron configurations. In the singlet Os–S, the Os–Os quintuple bond is of the type  $\sigma + 2\pi + 2\delta$  with one  $\sigma$  bond and two full two-electron  $\delta$  bonds. However, in triplet Os–T, the Os–Os quintuple bond is of the type  $2\sigma + 2\pi + \frac{1}{2}\delta$



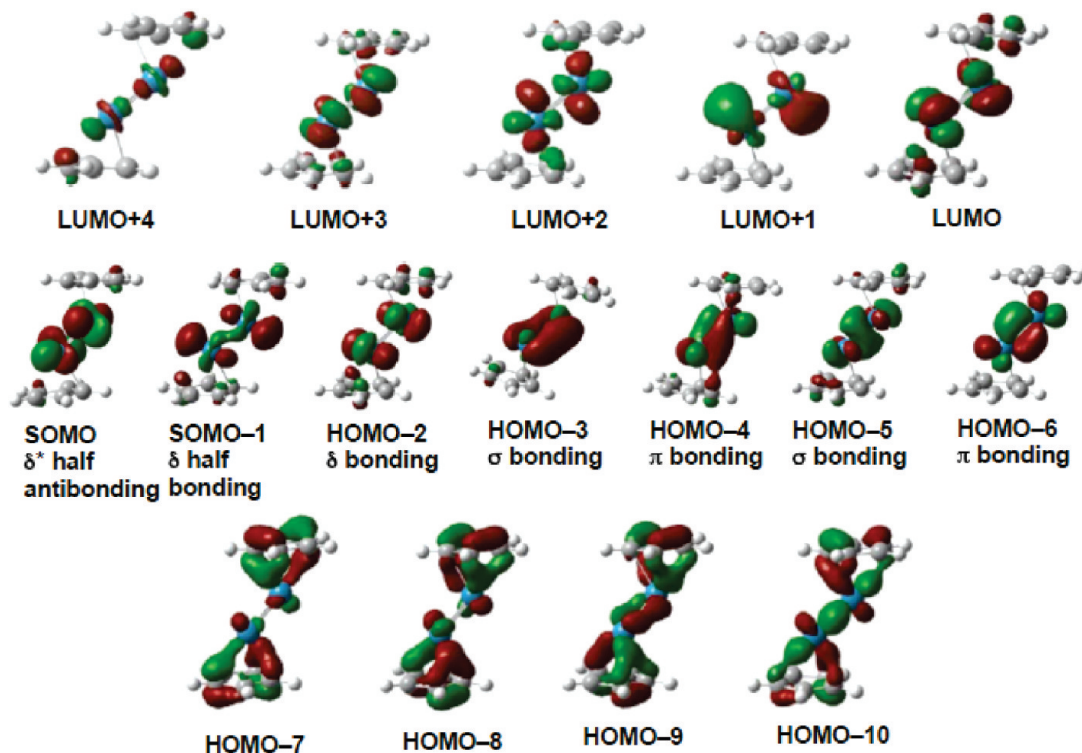


**Figure 8.** The frontier MOs for structure Re-T<sub>1</sub> of Cp<sub>2</sub>Re<sub>2</sub>. (a) Top: The unoccupied LUMO up to LUMO+4. (b) Middle: The occupied orbitals SOMO, SOMO-1, and HOMO-2 down to HOMO-6, relating to the rhenium-rhenium bonding. (c) Bottom: The next lower occupied MOs (HOMO-7 down to HOMO-10), relating largely to the metal-ring bonding.

with two  $\delta$  single electron “half” bonds and a second  $\sigma$  bond based on overlap of the  $d(z^2)$  orbitals. The predicted Os-Os distances for these two types of quintuple bonds are within 0.02 Å of each other, namely, 2.276 Å for the singlet Os-S and 2.255 Å for the triplet Os-T.

Dirhenocene, Cp<sub>2</sub>Re<sub>2</sub>, has two electrons less than dismocene Cp<sub>2</sub>Os<sub>2</sub>. In the singlet structure Re-S (Figure 3) for dirhenocene, the  $\sigma^*$  antibonding HOMO of Cp<sub>2</sub>Os<sub>2</sub> (Figure 6) is empty because of these “missing” two electrons. Therefore, the Re-Re bond in Re-S has six components, namely, two  $\pi$  components and four  $\sigma$  and  $\delta$  components. Because of the bending in Re-S, the  $\sigma$  and  $\delta$  components are not readily distinguishable. These six components of the Re-Re bond in Re-S imply that the sextuple bond required to give both rhenium atoms the favored 18-electron configuration. Thus, six of the nine orbitals in the  $sp^3d^5$  manifolds of each rhenium atom are allocated to the Re-Re sextuple bond leaving three orbitals on each metal atom for the  $\sigma + 2\pi$  components of the metal-ring bonds. A sextuple bond has been postulated for the bare dimers M<sub>2</sub> (M = Cr, Mo, W) of the group 6 metals.<sup>51</sup> Note that the  $d^6$  formal Re(I) in Cp<sub>2</sub>Re<sub>2</sub> is isoelectronic with the  $d^6$  formal M(0) in the group 6 metal dimers (considering the Cp ring as Cp<sup>-</sup> with the favorable 6  $\pi$  electrons). The formal sextuple bond in the Cp<sub>2</sub>Re<sub>2</sub> structure Re-S is consistent with its predicted  $2.22 \pm 0.03$  Å distance being  $\sim 0.08$  Å shorter than the formal Os-Os quintuple bond distance of  $2.30 \pm 0.03$  Å in the singlet Cp<sub>2</sub>Os<sub>2</sub> structure Os-S.

The lowest energy Cp<sub>2</sub>Re<sub>2</sub> structure by either method is not the singlet Re-S but the triplet Re-T<sub>1</sub>, which lies marginally lower in energy (Figure 3 and Table 2). The

frontier MOs of Re-T<sub>1</sub> are shown in Figure 8. The Re-T<sub>1</sub> SOMOs, like those in the triplet Cp<sub>2</sub>Os<sub>2</sub> structure Os-T discussed above, contain only a single electron, yielding triplet spin multiplicity. One of these half-filled orbitals (SOMO) is a  $\delta^*$  antibonding orbital, whereas the other half-filled orbital (SOMO-1) is a  $\delta$  bonding orbital. Thus, these two half-filled orbitals in Re-T<sub>1</sub> make no net contribution to the rhenium-rhenium bonding. The five orbitals below the SOMOs, namely HOMO-2 to HOMO-6, inclusive (Figure 8), all contain electron pairs and have most of their electron density on the rhenium atoms rather than the Cp rings. These five orbitals represent the five components of a Re-Re quintuple bond thereby giving both rhenium atoms the 17-electron configurations for a binuclear triplet. However, this Re-Re quintuple bond in Re-T<sub>1</sub> has  $\sigma(s) + \sigma(z^2) + 2\pi + \delta$  components rather than the  $\sigma(s) + 2\pi + 2\delta$  components of the Os-Os quintuple bond in Os-S (Figure 6). The formal quintuple bond in the Cp<sub>2</sub>Re<sub>2</sub> triplet Re-T<sub>1</sub> is consistent with the predicted Re-Re distance of  $2.30 \pm 0.03$  Å, which is essentially identical to the Os-Os quintuple bond distance in Os-S and longer than the Re-Re sextuple bond distance of  $2.22 \pm 0.03$  Å for singlet Re-S. The Re-T<sub>1</sub> orbitals below HOMO-6 (e.g., HOMO-7 through HOMO-10 in Figure 8) have most of their electron density on the Cp rings and thus may be related to the rhenium-ring bonding.

Dirungstenocene, Cp<sub>2</sub>W<sub>2</sub>, has two electrons less than dirhenocene. The lowest energy Cp<sub>2</sub>W<sub>2</sub> structure is the singlet W-S (Figure 4). The frontier MOs of W-S are shown in Figure 9. The five highest lying filled MOs (HOMO down to HOMO-4) have their electron densities concentrated on the metal-metal bond and are all bonding orbitals. This



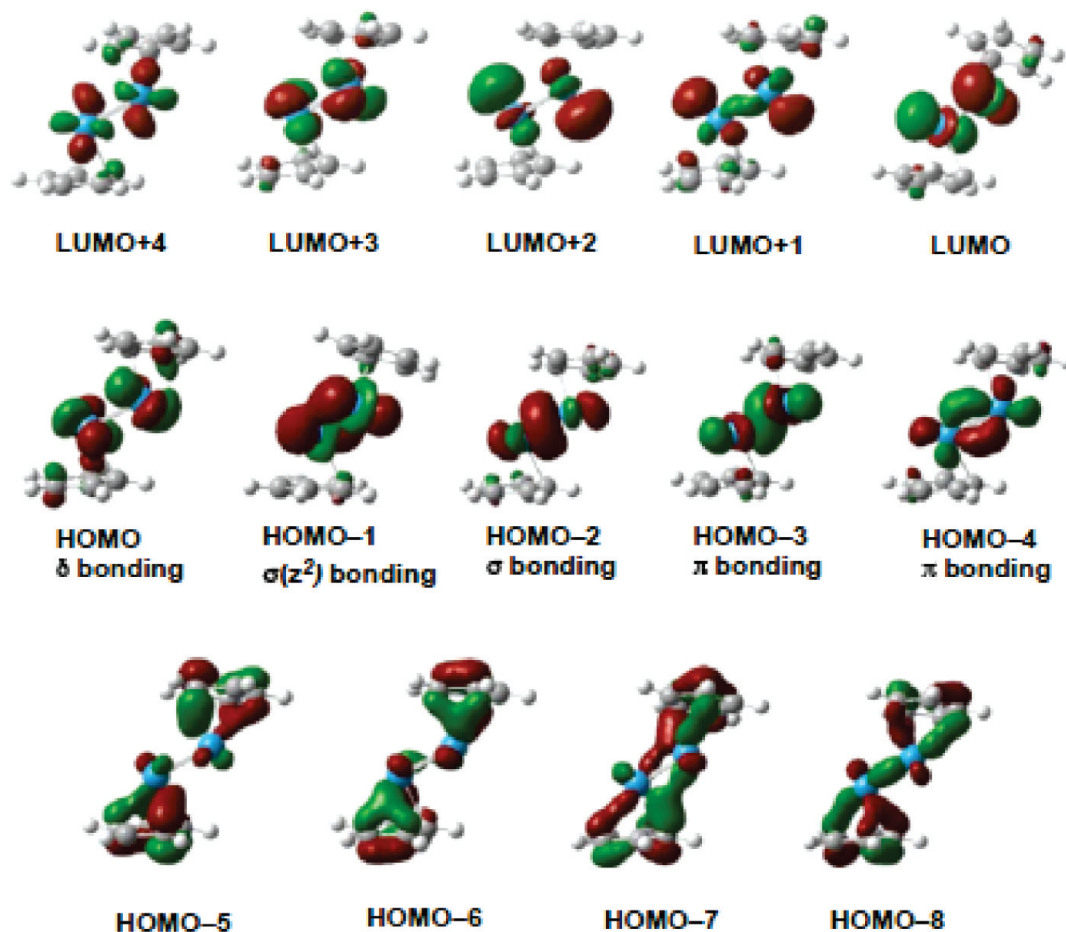


**Figure 9.** The frontier MOs for structure W–S of  $\text{Cp}_2\text{W}_2$ . (a) Top: The LUMOs up to LUMO+4. (b) Middle: The occupied HOMOs down to HOMO–4, relating to the tungsten–tungsten bonding. (c) Bottom: The next lower occupied MOs (HOMO–5 down to HOMO–8), relating largely to the metal–ring bonding.

indicates a formal quintuple W–W bond in W–S giving both tungsten atoms a 16-electron configuration. This quintuple bond has one  $\delta$  component (HOMO), two  $\sigma$  components (HOMO–1 and HOMO–2), and two  $\pi$  components (HOMO–3 and HOMO–4) and thus is similar to the Re–Re quintuple bond in the triplet  $\text{Cp}_2\text{Re}_2$  structure Re– $\text{T}_1$ . The predicted W–W quintuple bond distance in W–S of  $2.30 \pm 0.01 \text{ \AA}$  is essentially identical with the predicted metal–metal quintuple bond distances in the singlet  $\text{Cp}_2\text{Os}_2$  structure Os–S and the triplet  $\text{Cp}_2\text{Re}_2$  structure Re– $\text{T}_1$ .

Ditantalocene,  $\text{Cp}_2\text{Ta}_2$ , has two electrons less than ditungstocene. The frontier MOs of the lowest energy singlet  $\text{Cp}_2\text{Ta}_2$  structure Ta– $\text{S}_1$  are shown in Figure 10. The four highest lying filled MOs (HOMO down to HOMO–4) have their electron densities concentrated on the metal–metal bond and are all bonding orbitals. This indicates a formal quadruple Ta–Ta bond in Ta– $\text{S}_1$ . This quadruple bond has two  $\sigma$  components (HOMO and HOMO–3) and two  $\pi$  components (HOMO–1 and HOMO–2). Thus, the two electrons lost in going from singlet  $\text{Cp}_2\text{W}_2$  to singlet  $\text{Cp}_2\text{Ta}_2$  come from the  $\delta$  component of the metal–metal multiple bond. The reduction in the formal metal–metal bond order from five in singlet  $\text{Cp}_2\text{W}_2$  W–S to four in singlet  $\text{Cp}_2\text{Ta}_2$  Ta– $\text{S}_1$  is

consistent with a lengthening of the predicted metal–metal distance from  $2.30 \pm 0.01 \text{ \AA}$  in W–S to  $2.38 \pm 0.02 \text{ \AA}$  in Ta– $\text{S}_1$ .

#### 4. Discussion

Analysis of the metal–metal multiple bonding in the dimetalloenes uses the 18-electron rule and variations thereof to determine the formal metal–metal multiple bond orders. Thus, the singlet structures of  $\text{Cp}_2\text{Os}_2$  (Os–S in Figure 2) and  $\text{Cp}_2\text{Re}_2$  (Re–S in Figure 3) have the formal metal–metal bond orders of five and six required by the 18-electron rule. However, the lowest energy structure of  $\text{Cp}_2\text{Re}_2$  (Re– $\text{T}_1$  in Figure 3) is a triplet with a formal Re–Re bond order of five giving the rhenium atoms the 17-electron configurations required for a binuclear triplet. The triplet structure of  $\text{Cp}_2\text{Os}_2$  (Os–T in Figure 2) has the quintuple bond required to give both osmium atoms an 18-electron configuration. The triplet spin multiplicity in Os–T arises from the two unpaired electrons in the  $\delta$  components of the Os–Os bond, which are only “half bonds” with single electrons.

The 18-electron rule does not apply to the dimetalloenes of tungsten and tantalum, since the required bond orders of seven and eight require more bonding orbitals than are available, after considering the three orbitals required for the

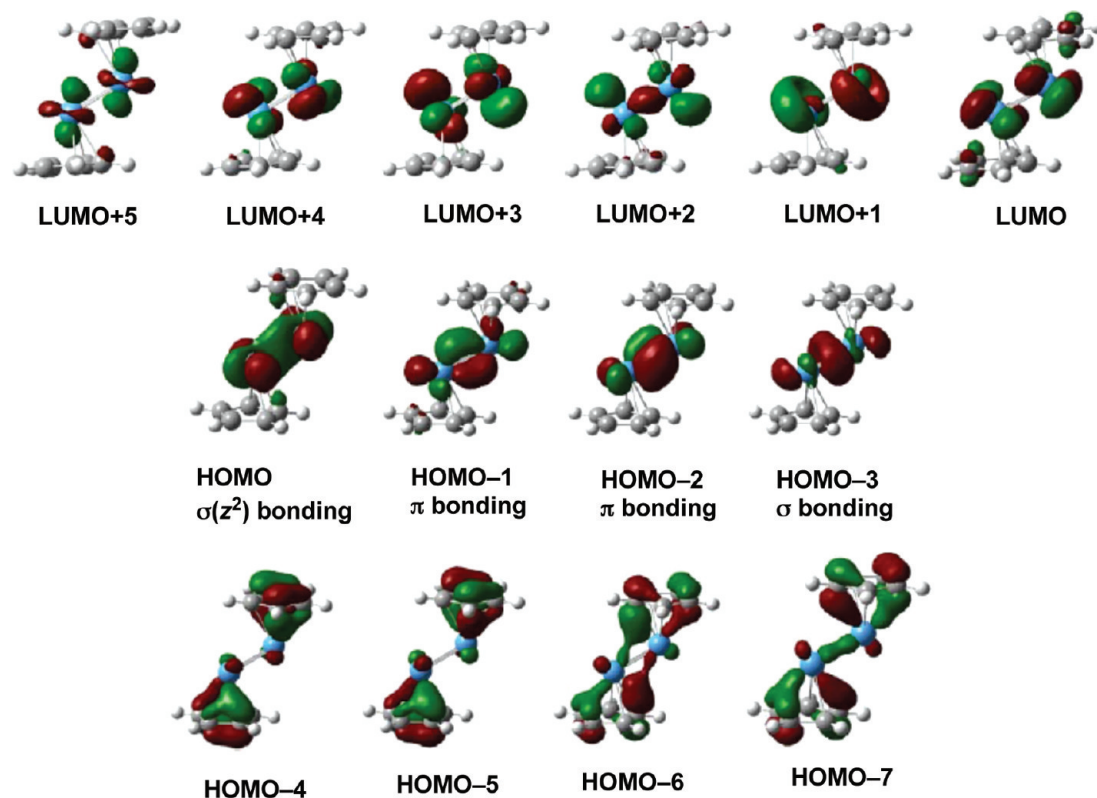


**Figure 10.** The frontier MOs for structure Ta-S<sub>1</sub> of Cp<sub>2</sub>Ta<sub>2</sub>. (a) Top: The LUMOs up to LUMO+5. (b) Middle: The HOMOs down to HOMO-3, relating to the Ta-Ta bonding. (c) Bottom: The next lower occupied MOs (HOMO-4 down to HOMO-7), relating largely to the metal-ring bonding.

metal-ring bonding. The W-W bond in singlet Cp<sub>2</sub>W<sub>2</sub> (W-S in Figure 4) is a formal quintuple bond, giving both tungsten atoms 16-electron configurations. The Ta-Ta bond in singlet Cp<sub>2</sub>Ta<sub>2</sub> is a formal quadruple bond giving both tantalum atoms the 14-electron configuration.

Metal-metal triple bonds are readily obtained in dimetallocene carbonyl chemistry, as indicated by the known stable compounds Cp<sub>2</sub>V<sub>2</sub>(CO)<sub>5</sub>,<sup>52,53</sup> Cp<sub>2</sub>M<sub>2</sub>(CO)<sub>4</sub> (M = Cr,<sup>54-56</sup> Mo<sup>57,58</sup>), and Cp<sub>2</sub>M'<sub>2</sub>(CO)<sub>3</sub> (M' = Mn,<sup>59</sup> Re<sup>60</sup>), all of which have formal M≡M triple bonds. Such M≡M triple bonds have one  $\sigma$  and two orthogonal  $\pi$  components, much like the C≡C triple bond in acetylene. In order to increase the formal metal-metal bond order above three, it is necessary to add either one or two  $\delta$  components or a second  $\sigma$  component constructed by overlap of d( $z^2$ ) orbitals. The original experimentally achieved examples of metal-metal quadruple and quintuple bonds, namely Re<sub>2</sub>Cl<sub>8</sub><sup>2-</sup> (ref 3) and ArylCrCrAryl (ref 4), respectively, supplement the  $\sigma + 2\perp\pi$  triple bond with one or two full  $\delta$  two-electron bonds, respectively. In this respect, the formal Os-Os quintuple bond in singlet Cp<sub>2</sub>Os<sub>2</sub> (Os-S in Figure 2) is of the same type, i.e.,  $\sigma + 2\pi + 2\delta$ , as the Cr-Cr quintuple bond in the Cr(I) aryl derivatives ArylCrCrAryl.<sup>4</sup>

The  $\delta$  components of metal-metal multiple bonds are rather weak, as indicated by the chemistry of compounds with metal-metal quadruple bonds,<sup>1</sup> as well as the overlap in the relevant bonding molecular orbitals. For example, visual inspection of the two  $\delta$  bonding orbitals HOMO-1 and HOMO-2 in singlet Cp<sub>2</sub>Os<sub>2</sub> (Os-S in Figure 2) clearly indicates weaker overlap than the corresponding  $\sigma$  and  $\pi$

bonds (HOMO-4, HOMO-5, and HOMO-6). In the formal W-W quintuple bond of the electron poorer singlet ditungstocene W-S (Figures 4 and 9), there is only one  $\delta$  component arising from the HOMO. The other component of this W-W quintuple bond is a second  $\sigma$  component from overlap of the d( $z^2$ ) orbitals (HOMO-1). In addition the formal Ta-Ta quadruple bond in singlet Ta-S (Figures 5 and 10) does not have any  $\delta$  components but consists of two  $\sigma$  components and two  $\pi$  components.

None of the dimetallocenes discussed in this paper have yet been synthesized. However, such dimetallocenes are potentially accessible by the dehalogenation of CpMX<sub>n</sub> derivatives by reagents such as alkali metals. In order to stabilize these highly unsaturated Cp<sub>2</sub>M<sub>2</sub> structures it might be necessary to introduce bulky substituents on the Cp rings in order to block further reactions of the metal-metal multiple bonds. Such strategies have been used to prepare unusual multiple bonds in main group element derivatives such as Ga≡Ga triple bonds in [RGa≡GaR]<sup>2-</sup> (R = bulky aryl ligand),<sup>61</sup> B=B double bonds in L→BH=BH←L,<sup>62</sup> and Si=Si double bonds in L→Si=Si←L (L = bulky carbene ligand).<sup>63</sup>

**Acknowledgment.** We are indebted to the 111 Project (B07012) and the National Natural Science Foundation (20873045) of China as well as the U.S. National Science Foundation (Grants CHE-0749868 and CHE-0716718) for support of this research.

**Supporting Information Available:** Tables S1-S5: Theoretical harmonic vibrational frequencies for Cp<sub>2</sub>M<sub>2</sub> (M

= Os, Re, W, Ta) using the BP86 method. Tables S6–S24: Theoretical Cartesian coordinates  $\text{Cp}_2\text{M}_2$  (M = Os, Re, W, Ta) using the MPW1PW91 method. Figures S1–S18: The frontier MOs for  $\text{Cp}_2\text{M}_2$  (M = Os, Re, W, Ta) using the BP86 method. This information is available free of charge via the Internet at <http://pubs.acs.org/>.

## References

- (1) Cotton, F. A.; Walton, R. A. *Multiple Bonds Between Metal Atoms*, 2nd Ed.; Clarendon: Oxford, 1993; pp 1–27.
- (2) Radius, U.; Breher, F. *Angew. Chem., Int. Ed.* **2006**, *45*, 3006.
- (3) Cotton, F. A.; Harris, C. B. *Inorg. Chem.* **1965**, *4*, 330–334.
- (4) Nguyen, T.; Sutton, A. D.; Brynda, M.; Fettingner, J. C.; Long, G. J.; Power, P. P. *Science* **2005**, *310*, 844.
- (5) Frenking, G. *Science* **2005**, *310*, 796.
- (6) Radius, U.; Breher, F. *Angew. Chem., Int. Ed.* **2006**, *45*, 3006.
- (7) Brynda, M.; Gagliardi, L.; Widmark, P.-O.; Power, P. P.; Roos, B. O. *Angew. Chem., Int. Ed.* **2006**, *45*, 3804.
- (8) Roos, B. O.; Borin, A. C.; Gagliardi, L. *Angew. Chem., Int. Ed.* **2007**, *46*, 1469.
- (9) Merino, G.; Donald, K. J.; D'Acchioli, J. S.; Hoffmann, R. *J. Am. Chem. Soc.* **2007**, *129*, 15295.
- (10) Brynda, M.; Gagliardi, L.; Roos, B. O. *Chem. Phys. Lett.* **2009**, *471*, 1.
- (11) Wagner, F. R.; Noor, A.; Kempe, R. *Nature Chem.* **2009**, *1*, 529.
- (12) La Macchia, G.; Gagliardi, L.; Power, P. P.; Brynda, M. *J. Am. Chem. Soc.* **2008**, *130*, 5104.
- (13) Wolf, R.; Ni, C.; Nguyen, T.; Brynda, M.; Long, G. J.; Sutton, A. D.; Fischer, R. C.; Fettingner, J. C.; Hellman, M.; Pu, L.; Power, P. P. *Inorg. Chem.* **2007**, *46*, 11277.
- (14) Tsai, Y.-C.; Hsu, C.-W.; Yu, J.-S. K.; Lee, G.-H.; Wang, Y.; Kuo, T.-S. *Angew. Chem., Int. Ed.* **2008**, *47*, 7250.
- (15) Hsu, C.-W.; Yu, J.-S. K.; Yen, C.-H.; Lee, G.-H.; Wang, Y.; Tsai, Y.-C. *Angew. Chem., Int. Ed.* **2008**, *47*, 9933.
- (16) Noor, A.; Wagner, F. R.; Kempe, R. *Angew. Chem. Int. Ed.* **2008**, *47*, 7246.
- (17) Kreisel, K. A.; Yap, G. P. A.; Dmitrenko, O.; Landis, C. R.; Theopold, K. H. *J. Am. Chem. Soc.* **2007**, *129*, 14162.
- (18) Resa, I.; Carmona, E.; Gutierrez-Puebla, E.; Monge, A. *Science* **2004**, *305*, 1136.
- (19) Wang, Y.; Quillan, B.; Wei, P.; Wang, H.; Yang, X.-J.; Xie, Y.; King, R. B.; Schleyer, P. v. R.; Schaefer, H. F., III; Robinson, G. H. *J. Am. Chem. Soc.* **2005**, *127*, 11944.
- (20) Xie, Y.; Schaefer, H. F., III; King, R. B. *J. Am. Chem. Soc.* **2005**, *127*, 2818.
- (21) Ehlers, A. W.; Frenking, G. *J. Am. Chem. Soc.* **1994**, *116*, 1514.
- (22) Delly, B.; Wrinn, M.; Lüthi, H. P. *J. Chem. Phys.* **1994**, *100*, 5785.
- (23) Li, J.; Schreckenbach, G.; Ziegler, T. *J. Am. Chem. Soc.* **1995**, *117*, 486.
- (24) Jonas, V.; Thiel, W. *J. Phys. Chem.* **1995**, *102*, 8474.
- (25) Barckholtz, T. A.; Bursten, B. E. *J. Am. Chem. Soc.* **1998**, *120*, 1926.
- (26) Niu, S.; Hall, M. B. *Chem. Rev.* **2000**, *100*, 353.
- (27) Macchi, P.; Sironi, A. *Coord. Chem. Rev.* **2003**, *238*, 383.
- (28) Buhl, M.; Kabrede, H. *J. Chem. Theory Comput.* **2006**, *2*, 1282.
- (29) Tonner, R.; Heydenrych, G.; Frenking, G. *J. Am. Chem. Soc.* **2008**, *130*, 8952.
- (30) Ziegler, T.; Autschbach, J. *Chem. Rev.* **2005**, *105*, 2695.
- (31) Waller, M. P.; Bühl, M.; Geethanakshmi, K. R.; Wang, D.; Thiel, W. *Chem.—Eur. J.* **2007**, *13*, 4723.
- (32) Hayes, P. G.; Beddie, C.; Hall, M. B.; Waterman, R.; Tilley, T. D. *J. Am. Chem. Soc.* **2006**, *128*, 428.
- (33) Bühl, M.; Reimann, C.; Pantazis, D. A.; Bredow, T.; Neese, F. *J. Chem. Theory Comput.* **2008**, *4*, 1449.
- (34) Besora, M.; Carreon-Macedo, J.-L.; Cowan, J.; George, M. W.; Harvey, J. N.; Portius, P.; Ronayne, K. L.; Sun, X.-Z.; Towrie, M. *J. Am. Chem. Soc.* **2009**, *131*, 3583.
- (35) Ye, S.; Tuttle, T.; Bill, E.; Simkhorich, L.; Gross, Z.; Thiel, W.; Neese, F. *Chem.—Eur. J.* **2008**, *14*, 10839.
- (36) Becke, A. D. *Phys. Rev. A* **1988**, *38*, 3098.
- (37) Perdew, J. P. *Phys. Rev. B* **1986**, *33*, 8822.
- (38) Adamo, C.; Barone, V. *J. Chem. Phys.* **1998**, *108*, 664.
- (39) Zhao, Y.; Pu, J.; Lynch, B. J.; Truhlar, D. G. *Phys. Chem. Chem. Phys.* **2004**, *6*, 673.
- (40) Perdew, J. P. In *Electronic Structure of Solids*, 1991 ed.; Ziesche, P., Esching, H., Eds.; Akademik Verlag: Berlin, 1991; p 11.
- (41) Zhao, S.; Wang, W.; Li, Z.; Liu, Z. P.; Fan, K.; Xie, Y.; Schaefer, H. F. *J. Chem. Phys.* **2006**, *124*, 184102.
- (42) Feng, X.; Gu, J.; Xie, Y.; King, R. B.; Schaefer, H. F. *J. Chem. Theory Comput.* **2007**, *3*, 1580.
- (43) Andrae, D.; Haussermann, U.; Dolg, M.; Stoll, H.; Preuss, H. *Theor. Chim. Acta* **1990**, *77*, 123.
- (44) Dunning, T. H. *J. Chem. Phys.* **1970**, *53*, 2823.
- (45) Huzinaga, S. *J. Chem. Phys.* **1965**, *42*, 1293.
- (46) Frisch, M. J.; Trucks, G. W.; Schlegel, H. B.; Scuseria, G. E.; Robb, M. A.; Cheeseman, J. R.; Montgomery, J. A., Jr.; Vreven, T.; Kudin, K. N.; Burant, J. C.; Millam, J. M.; Iyengar, S. S.; Tomasi, J.; Barone, V.; Mennucci, B.; Cossi, M.; Scalmani, G.; Rega, N.; Petersson, G. A.; Nakatsuji, H.; Hada, M.; Ehara, M.; Toyota, K.; Fukuda, R.; Hasegawa, J.; Ishida, M.; Nakajima, T.; Honda, Y.; Kitao, O.; Nakai, H.; Klene, M.; Li, X.; Knox, J. E.; Hratchian, H. P.; Cross, J. B.; Bakken, V.; Adamo, C.; Jaramillo, J.; Gomperts, R.; Stratmann, R. E.; Yazyev, O.; Austin, A. J.; Cammi, R.; Pomelli, C.; Ochterski, J. W.; Ayala, P. Y.; Morokuma, K.; Voth, G. A.; Salvador, P.; Dannenberg, J. J.; Zakrzewski, V. G.; Dapprich, S.; Daniels, A. D.; Strain, M. C.; Farkas, O.; Malick, D. K.; Rabuck, A. D.; Raghavachari, K.; Foresman, J. B.; Ortiz, J. V.; Cui, Q.; Baboul, A. G.; Clifford, S.; Cioslowski, J.; Stefanov, B. B.; Liu, G.; Liashenko, A.; Piskorz, P.; Komaromi, I.; Martin, R. L.; Fox, D. J.; Keith, T.; Al-Laham, M. A.; Peng, C. Y.; Nanayakkara, A.; Challacombe, M.; Gill, P. M. W.; Johnson, B.; Chen, W.; Wong, M. W.; Gonzalez, C.; Pople, J. A. *Gaussian 03*, Revision C.02; Gaussian, Inc.: Wallingford, CT, 2004.
- (47) Zhang, J.; Huang, K.-W.; Szalda, D. J.; Bullock, R. M. *Organometallics* **2006**, *25*, 2209.
- (48) Hoyano, J. K.; Graham, W. A. G. *Chem. Comm.* **1982**, 27.

- (49) Alvarez, M. A.; Garcia, M. E.; Riera, V.; Ruiz, M. A.; Falvello, L. R.; Bois, C. *Organometallics* **1997**, *16*, 354.
- (50) Cotton, F. A.; Frenz, B. A.; Etner, J. A.; Walton, R. A. *Inorg. Chem.* **1976**, *15*, 1630.
- (51) Barden, C. J.; Rienstra-Kiracole, J. C.; Schaefer, H. F. *J. Chem. Phys.* **2000**, *113*, 609, and references cited therein.
- (52) Cotton, F. A.; Kruczynski, L.; Frenz, B. A. *J. Organomet. Chem.* **1978**, *160*, 93.
- (53) Huffman, J. C.; Lewis, L. N.; Caulton, K. G. *Inorg. Chem.* **1980**, *19*, 2755.
- (54) Curtis, M. D.; Butler, W. M. *J. Organomet. Chem.* **1978**, *155*, 131.
- (55) King, R. B.; Efraty, A.; Douglas, W. M. *J. Organomet. Chem.* **1973**, *60*, 125.
- (56) Potenza, J.; Giordano, P.; Mastropaolo, D.; Efraty, A. *Inorg. Chem.* **1974**, *13*, 2540.
- (57) King, R. B.; Bisnette, M. B. *J. Organomet. Chem.* **1967**, *8*, 287.
- (58) Huang, J. S.; Dahl, L. F. *J. Organomet. Chem.* **1983**, *243*, 57.
- (59) Herrmann, W. A.; Serrano, R.; Weichmann, J. *J. Organomet. Chem.* **1983**, *246*, C57.
- (60) Hoyano, J. K.; Graham, W. A. G. *Chem. Comm.* **1982**, 27.
- (61) Su, J.; Li, X.-W.; Crittendon, R. C.; Robinson, G. H. *J. Am. Chem. Soc.* **1997**, *119*, 5471.
- (62) Wang, Y.; Quillian, B.; Wei, P.; Wannere, C. S.; Xie, Y.; King, R. B.; Schaefer, H. F.; Schleyer, P. R.; Robinson, G. H. *J. Am. Chem. Soc.* **2007**, *129*, 12412.
- (63) Wang, Y.; Xie, Y.; Wei, P.; King, R. B.; Schaefer, H. F., III; Schleyer, P. v. R.; Robinson, G. H. *Science* **2008**, *321*, 1069.

CT900564P